

An optimal linear fusion estimation algorithm of reduced dimension for \mathbb{T} -proper systems with multiple packet dropouts

Rosa M. Fernández-Alcalá ^{*} , José D. Jiménez-López , Nicolas Le Bihan , and Clive Cheong Took 

¹ Department of Statistics and Operations Research, University of Jaén, Paraje Las Lagunillas, 23071, Jaén, Spain; rmfernand@ujaen.es (R. M. F. -A.); jdomingo@ujaen.es (J. D. J. -L.)

² Department of Images and Signals, CNRS/GIPSA-Lab, 38402 Saint Martin d'He'eres Cedex, France; nicolas.le-bihan@gipsa-lab.grenoble-inp.fr (N. L. B.)

³ Department of Electronic Engineering, Royal Holloway, London, TW20 OEX, UK; Clive.CheongTook@rhul.ac.uk (C. C. T.)

^{*} Correspondence: rmfernand@ujaen.es (R. M. F. -A.); Tel. : +34-953-212-449

Abstract: This paper analyses the centralized fusion linear estimation problem in multi-sensor systems with multiple packet dropouts and correlated noises. Packet dropouts are modeled by independent Bernoulli distributed random variables. This problem is addressed in the tessarine domain under conditions of \mathbb{T}_1 and \mathbb{T}_2 properness, which entails a reduction in the dimension of the problem and, consequently, computational savings. The methodology proposed enables us to provide an optimal (in the least-mean-squares sense) linear fusion filtering algorithm for estimating the tessarine state with a lower computational cost than the conventional one devised in the real field. Simulation results illustrate the performance and advantages of the solution proposed in different settings.

Keywords: centralized fusion estimation; multi-sensor systems; packet dropouts; tessarine signal processing; \mathbb{T}_k properness.

1. Introduction

In sensor networks, the problem of estimating the state observed by multiple sensors has been analyzed extensively in recent decades due to the variety of applications they have in signal processing (see, e.g., [1–9]).

In networked systems, sensor failures, network congestion, communications interferences or noises can cause random packet dropouts in data transmissions and, consequently, it is possible that the measurements available for state estimation are not always updated. These packet dropouts can be described by stochastic parameter systems that define the strategy followed to compensate for packet loss [10–22].

For multi-sensor systems, the potential of fusion estimation techniques to produce consistent and accurate estimators has been demonstrated. Thus, these techniques have also been applied to multi-sensor systems with multiple packet dropouts, giving rise to centralized as well as distributed fusion estimation algorithms (see, e.g., [4,10,23–27]). In general, centralized fusion methodology yields optimal estimators, but the computational load involved can be a handicap in practical applications.

Alternatively, 4D hypercomplex-based signal processing has been satisfactorily applied as a dimension reduction approach in multi-sensor fusion estimation problems with uncertainties [28–35]. Effectively, the benefit of using hypercomplex algebras is twofold: firstly, they may provide a compact representation of multidimensional signals and a better insight into the structure of the problem than that provided by a traditional or real formalism, and secondly, the characterization of certain properness properties related to the vanishing of some correlation or pseudo correlation functions, makes the dimension of the processes

Citation: . An optimal linear fusion estimation algorithm of reduced dimension for \mathbb{T} -proper systems with multiple packet dropouts. *Sensors* **2023**, *1*, 0. <https://doi.org/>

Received: 14 March 2023

Revised: 13 April 2023

Accepted: 14 April 2023

Published: 17 April 2023

Copyright: © 2024 by the authors. Submitted to *Sensors* for possible open access publication under the terms and conditions of the Creative Commons Attribution (CC BY) license (<https://creativecommons.org/licenses/by/4.0/>).

involved may be reduced. Then, even though the optimal processing in the 4D hypercomplex field is the widely linear (WL) processing, which implies to work on a four-dimensional vector; under properness conditions, WL processing is equivalent to using a signal processing based on a vector of reduced dimension. Notice that there is not an algebra that always leads to the better solution, but the choice of the best algebra at each situation depends on the proper characteristics of the processes involved.

From among the different 4D hypercomplex structures, quaternions and, more recently, tessarines have been the most popular algebras used in signal processing. They are characterized by different multiplication rules that endorse them different algebraic properties of interest: on the one hand, quaternions are a noncommutative division algebra and, on the other hand, tessarines are a commutative non-division algebra. Nevertheless, the fact that they have zero divisors does not have a major effect on their practical applications. Recently, due to the advantage of working with commutative algebras, the multi-sensor fusion estimation problem for systems with uncertain measurements has been addressed for tessarine signals with properness properties. Specifically, under \mathbb{T}_1 and \mathbb{T}_2 properness conditions, Kalman filter-like centralized and distributed fusion estimation algorithms have been proposed in [34,35] by considering different uncertainty situations (missing measurements and/or random delays), as well as correlated noises. The main interest of these algorithms lies in the reduction of the computational burden they entail under properness conditions, as achieving this computational saving from a real formalism is not possible. Nevertheless, the benefits of this methodology still have not been exploited in multiple sensor stochastic systems with packet dropouts.

This paper deals with the linear least-mean-squares (LLMS) fusion filtering problem for multi-sensor \mathbb{T}_k -proper, ($k = 1, 2$) tessarine systems with multiple packet dropouts. At each sensor, the multiple packet dropouts are described by independent Bernoulli distributed tessarine random vectors that, at any instant of time t , indicates whether the measurement output is received or lost, and in this second situation, the latest measurement available is used. Moreover, our formulation of the problem includes a possible correlation between the state and measurement noises. In this setting, using centralized fusion Kalman filter technique, and based on a \mathbb{T}_k -proper signal processing, an optimal linear fusion filtering algorithm of reduced dimension is provided for estimating the state as well as its mean squared error. Additionally, the performance of the solution proposed and its superiority over its counterpart in the quaternion domain is experimentally analyzed for the cases of \mathbb{T}_1 -properness as well as \mathbb{T}_2 -properness, by using a numerical example. In summary, the challenges of this paper are described in brief by the following items: 1) to address the LLMS fusion filtering problem for multisensor systems with multiple packet dropouts and correlated noises in the tessarine domain, 2) to establish conditions on the state space system that guarantee the \mathbb{T}_k -properness of the processes involved, 3) to analyze the implications of \mathbb{T}_k -properness in the reduction of the dimension of the problem, 4) to derive a recursive algorithm to obtain the optimal fusion filters, 5) to illustrate numerically the benefits of the proposed solution over their counterparts in the quaternion setting, under \mathbb{T}_k -properness conditions.

The paper is organized as follows: In Section 2 the main concepts and properties in the tessarine domain are reviewed. Specifically, a tessarine random signal vector is defined, its conjugations, the real and augmented vectors, the *pseudo* auto and cross correlation functions, the \mathbb{T}_k -properness, and the \star product between tessarines. Section 3 describes the centralized fusion filtering problem for multi-sensor systems with multiple packet dropouts and its formulation in the tessarine domain under conditions of \mathbb{T}_k -properness. On the basis of the state-space model of the tessarine signal and the observations, the WL stacked state-space system is built from the augmented vectors of the processes involved and, afterwards, under \mathbb{T}_k -properness conditions, an equivalent form of reduced dimension for the available observation equation is presented. Next, the \mathbb{T}_k -proper centralized linear fusion filtering algorithm based on Kalman filter techniques is presented in Section 4. Note that, to preserve the continuity of exposition, the derivation of the formulas of this algorithm

has been deferred to Appendix A. In Section 5, two numerical examples, one of them over simulated values, and the other one on a realistic phenomena, illustrate the theoretical results obtained. The paper finishes with the concluding remarks in Section 6.

1.1. Notations

The following standard notation is used throughout this paper: scalars are denoted by lightface letters, while boldface lowercase and boldface uppercase letters represent the vectors and matrices, respectively. The symbol $\mathbf{0}_{n \times m}$ (respectively, $\mathbf{0}_n$) stands for the $n \times m$ matrix (respectively, n column vector) whose all elements are zeros, \mathbf{I}_n is the $n \times n$ identity matrix, and $\mathbf{1}_n$ denotes the n column vector of ones.

\mathbb{Z} , \mathbb{R} and \mathbb{T} denote, respectively, the set of integer, real, and tessarine numbers. \mathbb{R}^n (respectively, \mathbb{T}^n) is the set of all n -dimensional real (respectively, tessarine) vectors, and $\mathbb{R}^{n \times m}$ (respectively, $\mathbb{T}^{n \times m}$) refers to the set of all $n \times m$ -dimensional real (respectively, tessarine) matrices. Moreover, the superscripts “*”, “T”, and “H” symbolize the tessarine conjugate, transpose, and Hermitian transpose, respectively.

The notation $E[\cdot]$ represents the mathematical expectation, $\text{Cov}(\cdot)$ is the covariance operator, and $\text{diag}(\cdot)$ denotes the diagonal (or block diagonal) matrix with the input arguments on the main diagonal. Finally, $\delta_{t,s}$ represents the Kronecker delta function, and the Hadamard and Kronecker product operators are symbolized by “o” and “ \otimes ”, respectively.

2. Definitions and Preliminaries

This section is devoted to stating the core concepts and results in the tessarine domain that will be used throughout the paper.

Unless otherwise indicated, we shall assume that all random variables have zero mean.

Definition 1. A tessarine random signal vector $\mathbf{x}(t) \in \mathbb{T}^n$ is a four-dimensional hypercomplex stochastic process defined as [36]

$$\mathbf{x}(t) = \mathbf{x}_r(t) + \eta \mathbf{x}_\eta(t) + \eta' \mathbf{x}_{\eta'}(t) + \eta'' \mathbf{x}_{\eta''}(t), \quad t \in \mathbb{Z},$$

with $\mathbf{x}_\nu(t) \in \mathbb{R}^n$, for $\nu = r, \eta, \eta', \eta''$, and where $\{\eta, \eta', \eta''\}$ are hyper-imaginary units such that:

$$\eta\eta' = \eta'', \quad \eta'\eta'' = \eta, \quad \eta''\eta = -\eta', \quad \eta^2 = \eta'^2 = -1, \quad \eta'^2 = 1.$$

Consider $\mathbf{x}(t), \mathbf{y}(t) \in \mathbb{T}^n$, tessarine random signal vectors given in Definition 1. The following concepts and properties can be established. Let $\mathbf{\Gamma}_\mathbf{x}(t, s) = E[\mathbf{x}(t)\mathbf{x}^H(s)]$ be the *pseudo* autocorrelation function of $\mathbf{x}(t) \in \mathbb{T}^n$, and $\mathbf{\Gamma}_{\mathbf{xy}}(t, s) = E[\mathbf{x}(t)\mathbf{y}^H(s)]$ the *pseudo* cross-correlation function of $\mathbf{x}(t), \mathbf{y}(t) \in \mathbb{T}^n$, $\forall t, s \in \mathbb{Z}$.

In the tessarine domain, the second-order statistical properties of $\mathbf{x}(t) \in \mathbb{T}^n$, are completely described from the augmented tessarine signal vector

$$\bar{\mathbf{x}}(t) = [\mathbf{x}^T(t), \mathbf{x}^{*T}(t), \mathbf{x}^{\eta T}(t), \mathbf{x}^{\eta' T}(t)]^T, \quad (1)$$

where $\mathbf{x}^*(t)$ is the conjugate of $\mathbf{x}(t)$ defined as

$$\mathbf{x}^*(t) = \mathbf{x}_r(t) - \eta \mathbf{x}_\eta(t) + \eta' \mathbf{x}_{\eta'}(t) - \eta'' \mathbf{x}_{\eta''}(t),$$

and

$$\mathbf{x}^\eta(t) = \mathbf{x}_r(t) + \eta \mathbf{x}_\eta(t) - \eta' \mathbf{x}_{\eta'}(t) - \eta'' \mathbf{x}_{\eta''}(t),$$

$$\mathbf{x}^{\eta''}(t) = \mathbf{x}_r(t) - \eta \mathbf{x}_\eta(t) - \eta' \mathbf{x}_{\eta'}(t) + \eta'' \mathbf{x}_{\eta''}(t).$$

Let $\mathbf{x}^r(t) = [\mathbf{x}_r^T(t), \mathbf{x}_\eta^T(t), \mathbf{x}_{\eta'}^T(t), \mathbf{x}_{\eta''}^T(t)]^T$ be the real vector formed by the components $\mathbf{x}_\nu(t) \in \mathbb{R}^n$, $\nu = r, \eta, \eta', \eta''$, of $\mathbf{x}(t) \in \mathbb{T}^n$. The following relationship can be established:

$$\bar{\mathbf{x}}(t) = 2\mathcal{T}\mathbf{x}^r(t),$$

where $\mathcal{T} = \frac{1}{2}\mathcal{A} \otimes \mathbf{I}_n$, with

$$\mathcal{A} = \begin{bmatrix} 1 & \eta & \eta' & \eta'' \\ 1 & -\eta & \eta' & -\eta'' \\ 1 & \eta & -\eta' & -\eta'' \\ 1 & -\eta & -\eta' & \eta'' \end{bmatrix}.$$

Notice that $\mathcal{T}^H \mathcal{T} = \mathbf{I}_{4n}$.

It should be highlighted that the properness profile of a tessarine random signal plays a key role in the choice of the suitable type of linear processing that leads to a reduction in the dimension of the problem. This properness profile is characterized by the degree of correlation between the imaginary components and the real component. In particular, two interesting types of properness can be defined in the tessarine domain [36,37].

Definition 2. Let $\mathbf{x}(t) \in \mathbb{T}^n$ be a tessarine random signal vector. It is said that:

- $\mathbf{x}(t)$ is \mathbb{T}_1 -proper if, and only if, $\mathbf{\Gamma}_{\mathbf{x}\mathbf{x}^\nu}(t, s) = 0$, for $\nu = *, \eta, \eta'',$ and $\forall t, s \in \mathbb{Z}$,
- $\mathbf{x}(t)$ is \mathbb{T}_2 -proper if, and only if, $\mathbf{\Gamma}_{\mathbf{x}\mathbf{x}^\nu}(t, s) = 0$, for $\nu = \eta, \eta'',$ and $\forall t, s \in \mathbb{Z}$.

Likewise, let $\mathbf{x}(t) \in \mathbb{T}^{n_1}$ and $\mathbf{y}(t) \in \mathbb{T}^{n_2}$ be two tessarine random signal vectors. It is said that:

- $\mathbf{x}(t)$ and $\mathbf{y}(t)$ are cross \mathbb{T}_1 -proper, if, and only if, $\mathbf{\Gamma}_{\mathbf{x}\mathbf{y}^\nu}(t, s) = 0$, for $\nu = *, \eta, \eta'',$ and $\forall t, s \in \mathbb{Z}$,
- $\mathbf{x}(t)$ and $\mathbf{y}(t)$ are cross \mathbb{T}_2 -proper, if, and only if, $\mathbf{\Gamma}_{\mathbf{x}\mathbf{y}^\nu}(t, s) = 0$, for $\nu = \eta, \eta'',$ and $\forall t, s \in \mathbb{Z}$,
- $\mathbf{x}(t)$ and $\mathbf{y}(t)$ are jointly \mathbb{T}_k -proper, for $k = 1, 2$, if, and only if, they are \mathbb{T}_k -proper and cross \mathbb{T}_k -proper.

Remark 1. In the tessarine domain, the optimal linear processing, the widely linear (WL) processing, is based on augmented tessarine vector of dimension $4n$ of the form given in (1). Nevertheless, when \mathbb{T}_k -properness conditions are satisfied, the WL estimators coincides with the one obtained from a \mathbb{T}_k -proper linear processing, which uses only the information provided by the processes involved (case $k = 1$) or the $2n$ -dimensional augmented vector formed by the signal and its conjugate (case $k = 2$). In consequence, \mathbb{T}_k -properness means there is a significant reduction in the dimension of the processes involved [37].

Finally, a new product between two tessarine signal vectors is defined.

Definition 3. Consider $\mathbf{x}(t), \mathbf{y}(s) \in \mathbb{T}^n$. The product \star is defined by the expression

$$\mathbf{x}(t) \star \mathbf{y}(s) = \mathbf{x}_r(t) \circ \mathbf{y}_r(s) + \eta \mathbf{x}_\eta(t) \circ \mathbf{y}_\eta(s) + \eta' \mathbf{x}_{\eta'}(t) \circ \mathbf{y}_{\eta'}(s) + \eta'' \mathbf{x}_{\eta''}(t) \circ \mathbf{y}_{\eta''}(s).$$

Note that, given two random tessarine signal vectors $\mathbf{x}(t), \mathbf{y}(s) \in \mathbb{T}^n$, the augmented vector of $\mathbf{x}(t) \star \mathbf{y}(s)$ is $\overline{\mathbf{x}(t) \star \mathbf{y}(s)} = \mathcal{D}^{\mathbf{x}}(t) \bar{\mathbf{y}}(s)$, with $\mathcal{D}^{\mathbf{x}}(t) = \mathcal{T} \text{diag}(\mathbf{x}^r(t)) \mathcal{T}^H$.

3. Problem formulation

Let $\mathbf{x}(t) \in \mathbb{T}^n$ be an n -dimensional tessarine state vector which is assumed to be observed from R sensors perturbed by different additive noises according to the state-space model:

$$\begin{aligned} \mathbf{x}(t+1) &= \mathbf{F}_1(t) \mathbf{x}(t) + \mathbf{F}_2(t) \mathbf{x}^*(t) + \mathbf{F}_3(t) \mathbf{x}^\eta(t) + \mathbf{F}_4(t) \mathbf{x}^{\eta''}(t) + \mathbf{u}(t), \quad t \geq 0, \\ \mathbf{z}^{(i)}(t) &= \mathbf{x}(t) + \mathbf{v}^{(i)}(t), \quad t \geq 1, \quad i = 1, \dots, R, \end{aligned}$$

with

- $\mathbf{F}_j(t) \in \mathbb{T}^{n \times n}$, $j = 1, \dots, 4$: deterministic tessarine matrices.
- $\mathbf{u}(t) \in \mathbb{T}^n$: tessarine white noises with *pseudo* variances $\mathbf{Q}(t)$.

- $\mathbf{v}^{(i)}(t) \in \mathbb{T}^n$: tessarine white noises with *pseudo* variances $\mathbf{R}^{(i)}(t)$.
- $\mathbf{u}(t), \mathbf{v}^{(i)}(t)$ correlated with $\mathbf{\Gamma}_{\mathbf{uv}^{(i)}}(t, s) = \mathbf{S}^{(i)}(t)\delta_{t,s}$.
- $\mathbf{v}^{(i)}(t), \mathbf{v}^{(j)}(t)$ independent for any two sensors $i \neq j$.
- $\mathbf{x}(0)$ uncorrelated with $\mathbf{u}(t)$ and $\mathbf{v}^{(i)}(t)$, for $t \geq 0, i = 1, \dots, R$.
- $\mathbf{\Gamma}_{\mathbf{x}}(0, 0) = \mathbf{P}_0$.

The packets or measured outputs $\mathbf{z}^{(i)}(t)$ are assumed to be affected by random packet dropouts characterized by Bernoulli distributed random variables that can be described by the following model:

$$\mathbf{y}^{(i)}(t) = \gamma^{(i)}(t) \star \mathbf{z}^{(i)}(t) + (\mathbf{1}_n - \gamma^{(i)}(t)) \star \mathbf{y}^{(i)}(t-1), \quad t \geq 2; \quad (2)$$

for $i = 1, \dots, R$, with $\mathbf{y}^{(i)}(1) = \mathbf{z}^{(i)}(1)$, and the \star product given in Definition 3. Moreover, at each sensor $i = 1, \dots, R$, the tessarine random vector $\gamma^{(i)}(t) = [\gamma_1^{(i)}(t), \dots, \gamma_n^{(i)}(t)]^T \in \mathbb{T}^n$ is of the form $\gamma_j^{(i)}(t) = \gamma_{j,r}^{(i)}(t) + \eta\gamma_{j,\eta}^{(i)}(t) + \eta'\gamma_{j,\eta'}^{(i)}(t) + \eta''\gamma_{j,\eta''}^{(i)}(t)$, for $j = 1, \dots, n$, where $\gamma_{j,\nu}^{(i)}(t)$ are independent Bernoulli random variables with known probabilities $p_{j,\nu}^{(i)}(t)$, for $j = 1, \dots, n$ and $\nu = r, \eta, \eta', \eta''$, that indicates whether the corresponding component of the packet or measured output $\mathbf{z}^{(i)}(t)$ of sensor i is received at time t ($\gamma_{j,\nu}^{(i)}(t) = 1$) or it is lost and the latest received previously component, corresponding to the measured output $\mathbf{z}^{(i)}(t-1)$ is used at time t ($\gamma_{j,\nu}^{(i)}(t) = 0$). Additionally, $\gamma^{(i)}(t)$ and $\gamma^{(i)}(s)$ are assumed to be independent for $t \neq s$, and $\gamma^{(i)}(t)$ is independent of $\mathbf{x}(t), \mathbf{u}(t), \mathbf{v}^{(l)}(t)$ and $\gamma^{(l)}(t)$, for $i \neq l$, with $i, l = 1, \dots, R$.

Remark 2. Observe that model (2) always considers the latest measurement output received when the current measurement output is lost during transmission. Hence, this model can be used to describe multiple packet dropouts.

Remark 3. Under the hypothesis established for the Bernoulli random variables $\gamma_{j,\nu}^{(i)}(t)$, it is not difficult to check that

$$\begin{aligned} E[\gamma_{j_1,\nu_1}^{(i_1)}(t)\gamma_{j_2,\nu_2}^{(i_2)}(t)] &= \begin{cases} p_{j_1,\nu_1}^{(i_1)}(t), & \text{if } i_1 = i_2, j_1 = j_2, \nu_1 = \nu_2 \\ p_{j_1,\nu_1}^{(i_1)}(t)p_{j_2,\nu_2}^{(i_2)}(t), & \text{otherwise,} \end{cases} \\ E[(1 - \gamma_{j_1,\nu_1}^{(i_1)}(t))(1 - \gamma_{j_2,\nu_2}^{(i_2)}(t))] &= \begin{cases} 1 - p_{j_1,\nu_1}^{(i_1)}(t), & \text{if } i_1 = i_2, j_1 = j_2, \nu_1 = \nu_2 \\ (1 - p_{j_1,\nu_1}^{(i_1)}(t))(1 - p_{j_2,\nu_2}^{(i_2)}(t)), & \text{otherwise,} \end{cases} \\ E[\gamma_{j_1,\nu_1}^{(i_1)}(t)(1 - \gamma_{j_2,\nu_2}^{(i_2)}(t))] &= \begin{cases} 0, & \text{if } i_1 = i_2, j_1 = j_2, \nu_1 = \nu_2 \\ p_{j_1,\nu_1}^{(i_1)}(t)(1 - p_{j_2,\nu_2}^{(i_2)}(t)), & \text{otherwise,} \end{cases} \end{aligned}$$

for any $j_1, j_2 = 1, \dots, n$, $\nu_1, \nu_2 = r, \eta, \eta', \eta''$ and $i_1, i_2 = 1, \dots, R$.

In this setting, and based on the information supplied by the received measurements, our aim is to devise efficient algorithms for computing the WL centralized fusion estimators of the signal $\mathbf{x}(t)$, under the conditions of \mathbb{T}_k -properness, for $k = 1, 2$.

With the purpose of a WL processing, the $4n$ -dimensional augmented vectors are considered. Then, the centralized fusion estimation problem is addressed by applying the traditional estimation methods on the following WL stacked state-space system:

$$\bar{\mathbf{x}}(t+1) = \bar{\Phi}(t)\bar{\mathbf{x}}(t) + \bar{\mathbf{u}}(t), \quad t \geq 0, \quad (3)$$

$$\bar{\mathbf{z}}(t) = \bar{\mathbf{C}}\bar{\mathbf{x}}(t) + \bar{\mathbf{v}}(t), \quad t \geq 1, \quad (4)$$

$$\bar{\mathbf{y}}(t) = \bar{\mathcal{D}}^{\bar{\gamma}}(t)\bar{\mathbf{z}}(t) + \bar{\mathcal{D}}^{(1-\bar{\gamma})}(t)\bar{\mathbf{y}}(t-1), \quad t \geq 2, \quad (5)$$

with $\bar{\mathbf{y}}(1) = \bar{\mathbf{z}}(1)$, and where $\bar{\mathbf{z}}(t) = [\bar{\mathbf{z}}^{(1)\top}(t), \dots, \bar{\mathbf{z}}^{(R)\top}(t)]^\top$, $\bar{\mathbf{v}}(t) = [\bar{\mathbf{v}}^{(1)\top}(t), \dots, \bar{\mathbf{v}}^{(R)\top}(t)]^\top$, and $\bar{\mathbf{y}}(t) = [\bar{\mathbf{y}}^{(1)\top}(t), \dots, \bar{\mathbf{y}}^{(R)\top}(t)]^\top$. Moreover,

$$\bar{\Phi}(t) = \begin{bmatrix} \mathbf{F}_1(t) & \mathbf{F}_2(t) & \mathbf{F}_3(t) & \mathbf{F}_4(t) \\ \mathbf{F}_2^*(t) & \mathbf{F}_1^*(t) & \mathbf{F}_4^*(t) & \mathbf{F}_3^*(t) \\ \mathbf{F}_3^\eta(t) & \mathbf{F}_4^\eta(t) & \mathbf{F}_1^\eta(t) & \mathbf{F}_2^\eta(t) \\ \mathbf{F}_4^{\eta''}(t) & \mathbf{F}_3^{\eta''}(t) & \mathbf{F}_2^{\eta''}(t) & \mathbf{F}_1^{\eta''}(t) \end{bmatrix},$$

$\bar{\mathcal{D}}^{\bar{\gamma}}(t) = \mathbf{Y} \text{diag}(\bar{\gamma}^r(t)) \mathbf{Y}^H$, $\bar{\mathcal{D}}^{(1-\bar{\gamma})}(t) = \mathbf{Y} \text{diag}(\mathbf{1}_{4nR} - \bar{\gamma}^r(t)) \mathbf{Y}^H$, with $\mathbf{Y} = \mathbf{I}_R \otimes \mathcal{T}$ and $\bar{\gamma}^r(t) = [\gamma^{(1)r^\top}(t), \dots, \gamma^{(R)r^\top}(t)]^\top$, and $\mathcal{C} = \mathbf{1}_R \otimes \mathbf{I}_{4n}$.

Furthermore, $\Gamma_{\bar{\mathbf{u}}}(t, s) = \bar{\mathbf{Q}}(t) \delta_{t,s}$, $\Gamma_{\bar{\mathbf{v}}}(t, s) = \bar{\mathbf{R}}(t) \delta_{t,s}$, and $\Gamma_{\bar{\mathbf{u}}\bar{\mathbf{v}}}(t, s) = \bar{\mathbf{S}}(t) \delta_{t,s}$, where $\bar{\mathbf{R}}(t) = \text{diag}(\bar{\mathbf{R}}^{(1)}(t), \dots, \bar{\mathbf{R}}^{(R)}(t))$, with $\bar{\mathbf{R}}^{(i)}(t) = \Gamma_{\bar{\mathbf{v}}^{(i)}}(t, t)$, and $\bar{\mathbf{S}}(t) = [\bar{\mathbf{S}}^{(1)}(t), \dots, \bar{\mathbf{S}}^{(R)}(t)]$, with $\bar{\mathbf{S}}^{(i)}(t) = \Gamma_{\bar{\mathbf{u}}\bar{\mathbf{v}}^{(i)}}(t, t)$, for $i = 1, \dots, R$.

Now, the centralized fusion estimation problem is analyzed in a \mathbb{T}_k -properness setting. The following Proposition establishes conditions on system (3)-(5) that guarantee the \mathbb{T}_k -properness of the processes involved.

Proposition 1. *Given the WL stacked state-space model (3)-(5), and taking into account the \mathbb{T}_k -properness concepts given in Definition 2, the following properties can be established:*

1. $\mathbf{x}(t)$ is \mathbb{T}_1 -proper if and only if the initial state $\mathbf{x}(0)$ and the state noise $\mathbf{u}(t)$ are \mathbb{T}_1 -proper, and the matrix $\bar{\Phi}(t)$ is block diagonal as described below

$$\bar{\Phi}(t) = \text{diag}(\mathbf{F}_1(t), \mathbf{F}_1^*(t), \mathbf{F}_1^\eta(t), \mathbf{F}_1^{\eta''}(t)),$$

If additionally $\mathbf{v}^{(i)}(t)$ is \mathbb{T}_1 -proper, $\mathbf{u}(t)$ and $\mathbf{v}^{(i)}(t)$ are cross \mathbb{T}_1 -proper, and $p_{j,r}^{(i)}(t) = p_{j,\eta}^{(i)}(t) = p_{j,\eta'}^{(i)}(t) = p_{j,\eta''}^{(i)}(t) \triangleq p_j^{(i)}(t)$, $\forall t, j = 1, \dots, n, i = 1, \dots, R$, then $\mathbf{x}(t)$ and $\mathbf{y}^{(i)}(t)$ are jointly \mathbb{T}_1 -proper.

2. $\mathbf{x}(t)$ is \mathbb{T}_2 -proper if and only if the initial state $\mathbf{x}(0)$ and the state noise $\mathbf{u}(t)$ are \mathbb{T}_2 -proper, and the matrix $\bar{\Phi}(t)$ is block diagonal as described below

$$\bar{\Phi}(t) = \text{diag}(\Phi_2(t), \Phi_2^\eta(t)), \quad \text{with } \Phi_2(t) = \begin{bmatrix} \mathbf{F}_1(t) & \mathbf{F}_2(t) \\ \mathbf{F}_2^*(t) & \mathbf{F}_1^*(t) \end{bmatrix},$$

If additionally $\mathbf{v}^{(i)}(t)$ is \mathbb{T}_2 -proper, $\mathbf{u}(t)$ and $\mathbf{v}^{(i)}(t)$ are cross \mathbb{T}_2 -proper, and $p_{j,r}^{(i)}(t) = p_{j,\eta}^{(i)}(t)$, $p_{j,\eta'}^{(i)}(t) = p_{j,\eta''}^{(i)}(t)$, $\forall t, j = 1, \dots, n, i = 1, \dots, R$, then $\mathbf{x}(t)$ and $\mathbf{y}^{(i)}(t)$ are jointly \mathbb{T}_2 -proper.

Remark 4. *It should be observed that the conditions established in Proposition 1 for ensuring the different type of properness on the processes involved in (3)-(5), are similar to the one stated in [34].*

Then, under conditions of \mathbb{T}_k -properness, for $k = 1, 2$, the measurement equation (5) in the above WL stacked state-space model can be expressed in the following equivalent form of reduced dimension:

$$\mathbf{y}_k(t) = \bar{\mathcal{D}}_k^{\bar{\gamma}}(t) \bar{\mathbf{z}}(t) + \bar{\mathcal{D}}_k^{1-\bar{\gamma}} \bar{\mathbf{y}}(t-1), \quad t \geq 2, \quad (6)$$

with $\mathbf{y}_k(1) = \Delta_k \bar{\mathbf{z}}(1)$, and $\Delta_k = \mathbf{I}_R \otimes [\mathbf{I}_{kn}, \mathbf{0}_{kn \times (4-k)n}]$. Furthermore, $\mathcal{D}_k^{\bar{\gamma}}(t) = \mathbf{Y}_k \text{diag}(\bar{\gamma}^r(t)) \mathbf{Y}^H$ and $\mathcal{D}_k^{1-\bar{\gamma}}(t) = \mathbf{Y}_k \text{diag}(\mathbf{1}_{4nR} - \bar{\gamma}^r(t)) \mathbf{Y}^H$, where $\mathbf{Y}_k = \mathbf{I}_R \otimes \mathcal{T}_k$, with $\mathcal{T}_k = \frac{1}{2} \mathcal{B}_k \otimes \mathbf{I}_n$, and

$$\mathcal{B}_k = \begin{cases} \begin{bmatrix} 1 & \eta & \eta' & \eta'' \end{bmatrix}, & \text{for } k = 1 \\ \begin{bmatrix} 1 & \eta & \eta' & \eta'' \\ 1 & -\eta & \eta' & -\eta'' \end{bmatrix}, & \text{for } k = 2. \end{cases}$$

In addition,

$$\begin{aligned} \bar{\Pi}_k^{\bar{\gamma}}(t) &= E[\mathcal{D}_k^{\bar{\gamma}}(t)] = \text{diag}(\bar{\Pi}_k^{\gamma^{(1)}}(t), \dots, \bar{\Pi}_k^{\gamma^{(R)}}(t)), \\ \bar{\Pi}_k^{(1-\bar{\gamma})}(t) &= E[\mathcal{D}_k^{(1-\bar{\gamma})}(t)] = \text{diag}(\bar{\Pi}_k^{(1-\gamma^{(1)})}(t), \dots, \bar{\Pi}_k^{(1-\gamma^{(R)})}(t)), \end{aligned}$$

with $\bar{\Pi}_k^{\gamma^{(i)}}(t) = [\Pi_k^{(i)}(t), \mathbf{0}_{kn \times (4-k)n}]$ and $\bar{\Pi}_k^{(1-\gamma^{(i)})}(t) = [\mathbf{I}_{kn} - \Pi_k^{(i)}(t), \mathbf{0}_{kn \times (4-k)n}]$,

$$\begin{aligned} \Pi_1^{(i)}(t) &= \text{diag}(p_{1,r}^{(i)}(t), \dots, p_{n,r}^{(i)}(t)), \quad i = 1, \dots, R, \\ \Pi_2^{(i)}(t) &= \frac{1}{2} \begin{bmatrix} \Pi_a^{(i)}(t) & \Pi_b^{(i)}(t) \\ \Pi_b^{(i)}(t) & \Pi_a^{(i)}(t) \end{bmatrix}, \quad i = 1, \dots, R, \end{aligned} \quad (7)$$

and

$$\begin{aligned} \Pi_a^{(i)}(t) &= \text{diag}(p_{1,r}^{(i)}(t) + p_{1,\eta'}^{(i)}(t), \dots, p_{n,r}^{(i)}(t) + p_{n,\eta'}^{(i)}(t)), \quad i = 1, \dots, R, \\ \Pi_b^{(i)}(t) &= \text{diag}(p_{1,r}^{(i)}(t) - p_{1,\eta'}^{(i)}(t), \dots, p_{n,r}^{(i)}(t) - p_{n,\eta'}^{(i)}(t)), \quad i = 1, \dots, R. \end{aligned}$$

Remark 5. It is worth to note that \mathbb{T}_k -properness also allows to reduce the dimension of the equations (3) and (4) by replacing the $4n$ -dimensional augmented processes $\bar{\mathbf{x}}(t)$, $\bar{\mathbf{u}}(t)$, $\bar{\mathbf{z}}^{(i)}(t)$, $\bar{\mathbf{v}}^{(i)}(t)$, and the matrix $\bar{\Phi}(t)$ by the corresponding kn -dimensional vectors $\mathbf{x}_k(t)$, $\mathbf{u}_k(t)$, $\mathbf{z}_k^{(i)}(t)$, $\mathbf{v}_k^{(i)}(t)$ and $\Phi_k(t)$, defined as

- **\mathbb{T}_1 -proper case:** $\mathbf{x}_1(t) \triangleq \mathbf{x}(t)$, $\mathbf{u}_1(t) \triangleq \mathbf{u}(t)$, $\mathbf{z}_1^{(i)}(t) \triangleq \mathbf{z}^{(i)}(t)$, $\mathbf{v}_1^{(i)}(t) \triangleq \mathbf{v}^{(i)}(t)$ and $\Phi_1(t) \triangleq \Phi(t)$.
- **\mathbb{T}_2 -proper case:** $\mathbf{x}_2(t) \triangleq [\mathbf{x}(t), \mathbf{x}^H(t)]^T$, $\mathbf{u}_2(t) \triangleq [\mathbf{u}(t), \mathbf{u}^H(t)]^T$, $\mathbf{z}_2^{(i)}(t) \triangleq [\mathbf{z}^{(i)}(t), \mathbf{z}^{(i)H}(t)]^T$, $\mathbf{v}_2^{(i)}(t) \triangleq [\mathbf{v}^{(i)}(t), \mathbf{v}^{(i)H}(t)]^T$, and $\Phi_2(t)$ given in Proposition 1, in a \mathbb{T}_2 -proper scenario.

Furthermore, $\Gamma_{\mathbf{u}_k}(t, s) = \mathbf{Q}_k(t) \delta_{t,s}$, $\Gamma_{\mathbf{v}_k^{(i)}}(t, s) = \mathbf{R}_k^{(i)}(t) \delta_{t,s}$, $\Gamma_{\mathbf{u}_k \mathbf{v}_k^{(i)}}(t, s) = \mathbf{S}_k^{(i)}(t) \delta_{t,s}$, and $\Gamma_{\mathbf{x}_k}(0, 0) = \mathbf{P}_{0_k}$.

Thus, whereas the optimal linear processing in the tessarine domain suggests computing the LLMS filter of the state $\mathbf{x}(t) \in \mathbb{T}^n$ from its projection onto the augmented measurements $\{\bar{\mathbf{y}}(1), \dots, \bar{\mathbf{y}}(t)\}$, under conditions of \mathbb{T}_k -properness, for $k = 1, 2$, this estimator can be obtained from the measurements $\{\mathbf{y}_k(1), \dots, \mathbf{y}_k(t)\}$ defined in (6), which gives rise to the so-called \mathbb{T}_k -proper estimators. This approach supposes a reduction in the dimension of the problem that leads to computational savings that cannot be attained from a real formalism.

This methodology has been recently applied to design recursive fusion estimation algorithms for multi-sensor systems affected by random delays and missing measurements [35]. In this paper, we are interested in extending this methodology to systems affected by random multiple-packet dropouts.

4. \mathbb{T}_k proper centralized fusion filtering estimation

In this section, based on Kalman filter techniques, an efficient algorithm is provided for the computation of the \mathbb{T}_k -proper LLMS centralized fusion filter $\hat{\mathbf{x}}^{\mathbb{T}_k}(t|t)$, for $k = 1, 2$, of the state $\mathbf{x}(t)$ described by the state-space system with packet dropouts given by the

equations (3)-(4), and (6), as well as its associated error *pseudo* covariance matrix $\mathbf{P}^{\mathbb{T}_k}(t|t)$. For this purpose, a recursive algorithm is devised under \mathbb{T}_k -properness conditions for the projection of $\bar{\mathbf{x}}(t)$ onto the set of measurements $\{\mathbf{y}_k(1), \dots, \mathbf{y}_k(t)\}$, denoted by $\hat{\mathbf{x}}_k(t|t)$, and its error *pseudo* covariance matrix $\mathbf{P}_k(t|t)$. Then, $\hat{\mathbf{x}}^{\mathbb{T}_k}(t|t)$ and $\mathbf{P}^{\mathbb{T}_k}(t|t)$ are determined by the first n components of $\hat{\mathbf{x}}_k(t|t)$ and $\mathbf{P}_k(t|t)$, respectively.

Theorem 1 summarizes the formulas of this \mathbb{T}_k -proper LLMS centralized fusion filtering algorithm.

Theorem 1. *The \mathbb{T}_k -proper LLMS centralized fusion filter, $\hat{\mathbf{x}}^{\mathbb{T}_k}(t|t)$, for $k = 1, 2$, is obtained as follows*

$$\begin{aligned}\hat{\mathbf{x}}^{\mathbb{T}_1}(t|t) &= \hat{\mathbf{x}}_1(t|t), \\ \hat{\mathbf{x}}^{\mathbb{T}_2}(t|t) &= [\mathbf{1}_n, \mathbf{0}_n] \hat{\mathbf{x}}_2(t|t),\end{aligned}$$

where, for $k = 1, 2$, $\hat{\mathbf{x}}_k(t|t)$ is calculated from the recursive equation

$$\hat{\mathbf{x}}_k(t|t) = \hat{\mathbf{x}}_k(t|t-1) + \mathbf{L}_k(t) \boldsymbol{\epsilon}_k(t), \quad t \geq 1, \quad (8)$$

and $\hat{\mathbf{x}}_k(t+1|t)$ satisfies the recursive expression

$$\hat{\mathbf{x}}_k(t+1|t) = \boldsymbol{\Phi}_k(t) \hat{\mathbf{x}}_k(t|t) + \mathbf{H}_k(t) \boldsymbol{\epsilon}_k(t), \quad t \geq 1, \quad (9)$$

with initial values $\hat{\mathbf{x}}_k(1|0) = \hat{\mathbf{x}}_k(0|0) = \mathbf{0}_{kn}$.

The innovations $\boldsymbol{\epsilon}_k(t)$ are recursively calculated from the formula

$$\boldsymbol{\epsilon}_k(t) = \mathbf{y}_k(t) - \boldsymbol{\Pi}_k(t) \mathbf{C}_k \hat{\mathbf{x}}_k(t|t-1) - (\mathbf{I}_{knR} - \boldsymbol{\Pi}_k(t)) \mathbf{y}_k(t-1), \quad t \geq 2, \quad (10)$$

with initial value $\boldsymbol{\epsilon}_k(1) = \mathbf{y}_k(1)$, and $\mathbf{C}_k = \mathbf{1}_R \otimes \mathbf{I}_{kn}$.

Moreover, $\mathbf{H}_k(t) = \mathbf{S}_k(t) \boldsymbol{\Pi}_k(t) \boldsymbol{\Omega}_k^{-1}(t)$, where $\mathbf{S}_k(t) = [\mathbf{S}_k^{(1)}(t), \dots, \mathbf{S}_k^{(R)}(t)]$, and $\boldsymbol{\Pi}_k(t) = \text{diag}(\boldsymbol{\Pi}_k^{(1)}(t), \dots, \boldsymbol{\Pi}_k^{(R)}(t))$, with $\boldsymbol{\Pi}_k^{(i)}(t)$ given in (7). $\mathbf{L}_k(t) = \boldsymbol{\Theta}_k(t) \boldsymbol{\Omega}_k^{-1}(t)$, where the matrices $\boldsymbol{\Theta}_k(t)$ is obtained from the equation

$$\begin{aligned}\boldsymbol{\Theta}_k(t) &= \mathbf{P}_k(t|t-1) \mathbf{C}_k^T \boldsymbol{\Pi}_k(t), \quad t \geq 2; \\ \boldsymbol{\Theta}_k(1) &= \mathbf{1}_R^T \otimes \mathbf{D}_k(1),\end{aligned} \quad (11)$$

with

$$\mathbf{D}_k(1) = \left[\mathbf{I}_{kn}, \mathbf{0}_{kn \times (4-k)n} \right] \boldsymbol{\Gamma}_{\bar{\mathbf{x}}}(1, 1) \left[\mathbf{I}_{kn}, \mathbf{0}_{kn \times (4-k)n} \right]^T, \quad (12)$$

and where $\boldsymbol{\Gamma}_{\bar{\mathbf{x}}}(t, t)$ is given by the recursive expression

$$\boldsymbol{\Gamma}_{\bar{\mathbf{x}}}(t, t) = \bar{\boldsymbol{\Phi}}(t-1) \boldsymbol{\Gamma}_{\bar{\mathbf{x}}}(t-1, t-1) \bar{\boldsymbol{\Phi}}^H(t-1) + \bar{\mathbf{Q}}(t-1), \quad t \geq 1; \quad \boldsymbol{\Gamma}_{\bar{\mathbf{x}}}(0, 0) = \bar{\mathbf{P}}_0. \quad (13)$$

In addition,

$$\begin{aligned}\boldsymbol{\Omega}_k(t) &= \mathbf{Y}_k \left\{ \text{Cov}(\tilde{\boldsymbol{\gamma}}^r(t)) \circ (\boldsymbol{\Psi}_1(t) - \boldsymbol{\Psi}_2(t) - \boldsymbol{\Psi}_2^H(t) + \boldsymbol{\Psi}_3(t)) \right\} \mathbf{Y}_k^H \\ &\quad + \mathbf{Y}_k \left\{ \boldsymbol{\Gamma}_{\tilde{\boldsymbol{\gamma}}^r}(t, t) \circ (\mathbf{Y}^H \tilde{\mathbf{R}}(t) \mathbf{Y}) \right\} \mathbf{Y}_k^H + \boldsymbol{\Pi}_k(t) \mathbf{C}_k \mathbf{P}_k(t|t-1) \mathbf{C}_k^T \boldsymbol{\Pi}_k(t),\end{aligned} \quad (14)$$

where

$$\begin{aligned}\boldsymbol{\Psi}_1(t) &= \mathbf{Y}^H \mathbf{C} \boldsymbol{\Gamma}_{\bar{\mathbf{x}}}(t, t) \mathbf{C}^T \mathbf{Y}, \\ \boldsymbol{\Psi}_2(t) &= \mathbf{Y}^H \mathbf{C} \left(\bar{\boldsymbol{\Phi}}(t-1) \boldsymbol{\Gamma}_{\bar{\mathbf{x}}\bar{\mathbf{y}}}(t-1, t-1) + \bar{\mathbf{S}}(t-1) \bar{\boldsymbol{\Pi}}^{\tilde{\gamma}}(t-1) \right) \mathbf{Y}, \\ \boldsymbol{\Psi}_3(t) &= \mathbf{Y}^H \boldsymbol{\Gamma}_{\bar{\mathbf{y}}}(t-1, t-1) \mathbf{Y},\end{aligned}$$

with $\Gamma_{\bar{x}}(t, t)$ computed in (13),

$$\begin{aligned}\Gamma_{\bar{x}\bar{y}}(t, t) &= \Gamma_{\bar{x}}(t, t)\mathcal{C}^T\bar{\Pi}^{\bar{\gamma}}(t) + \left(\bar{\Phi}(t-1)\Gamma_{\bar{x}\bar{y}}(t-1, t-1) + \bar{\mathbf{S}}(t-1)\bar{\Pi}^{\bar{\gamma}}(t-1)\right)\bar{\Pi}^{1-\bar{\gamma}}(t), \quad t \geq 2; \\ \Gamma_{\bar{x}\bar{y}}(1, 1) &= \Gamma_{\bar{x}}(t, t)\mathcal{C}^T,\end{aligned}$$

and

$$\begin{aligned}\Gamma_{\bar{y}}(t, t) &= \mathbf{Y}\left\{\Gamma_{\bar{\gamma}^r}(t, t) \circ \left(\Psi_1(t) + \mathbf{Y}^H\bar{\mathbf{R}}(t)\mathbf{Y}\right) + \Gamma_{\bar{\gamma}^r(1-\bar{\gamma}^r)}(t, t) \circ \Psi_2(t) + \Gamma_{\bar{\gamma}^r(1-\bar{\gamma}^r)}^T(t, t) \circ \Psi_2^H(t) \right. \\ &\quad \left. + \Gamma_{(1-\bar{\gamma}^r)}(t, t) \circ \Psi_3(t)\right\}\mathbf{Y}^H, \quad t \geq 2; \\ \Gamma_{\bar{y}}(1, 1) &= \mathcal{C}\Gamma_{\bar{x}}(t, t)\mathcal{C}^T + \bar{\mathbf{R}}(1).\end{aligned}$$

Finally, the \mathbb{T}_k -proper centralized fusion filtering error pseudo covariance matrix, $\mathbf{P}^{\mathbb{T}_k}(t|t)$, for $k = 1, 2$, is obtained as follows:

$$\begin{aligned}\mathbf{P}^{\mathbb{T}_1}(t|t) &= \mathbf{P}_1(t|t), \\ \mathbf{P}^{\mathbb{T}_2}(t|t) &= [\mathbf{1}_n, \mathbf{0}_n]\mathbf{P}_2(t|t)[\mathbf{1}_n, \mathbf{0}_n]^T,\end{aligned}$$

where, for $k = 1, 2$, $\mathbf{P}_k(t|t)$ satisfies the following recursive equation:

$$\mathbf{P}_k(t|t) = \mathbf{P}_k(t|t-1) - \mathbf{\Theta}_k(t)\mathbf{\Omega}_k^{-1}(t)\mathbf{\Theta}_k^H(t), \quad (15)$$

with initial condition $\mathbf{P}_k(0|0) = \mathbf{P}_{0_k}$, and

$$\begin{aligned}\mathbf{P}_k(t+1|t) &= \mathbf{\Phi}_k(t)\mathbf{P}_k(t|t)\mathbf{\Phi}_k^H(t) - \mathbf{\Phi}_k(t)\mathbf{\Theta}_k(t)\mathbf{H}_k^H(t) - \mathbf{H}_k(t)\mathbf{\Theta}_k^H(t)\mathbf{\Phi}_k^H(t) \\ &\quad - \mathbf{H}_k(t)\mathbf{\Omega}_k(t)\mathbf{H}_k^H(t) + \mathbf{Q}_k(t),\end{aligned} \quad (16)$$

with initial condition $\mathbf{P}_k(1|0) = \mathbf{D}_k(1)$.

Remark 6. Notice that the computational load of the \mathbb{T}_k -proper LLMS centralized fusion filtering algorithms, for $k = 1, 2$, given in Theorem 1 is the same as that of their quaternion domain counterparts, i.e., those derived by using a quaternion strictly linear (QSL) and quaternion semi-widely linear (QSWL) processing, respectively.

As a consequence, it is noteworthy to see that the proposed \mathbb{T}_k -proper LLMS centralized fusion filtering algorithm provides estimations of the state that is equivalent to the one obtained from a WL processing or a real vectorial processing, whereas the computational load implied is reduced from $\mathcal{O}(64R^3n^3)$ to $\mathcal{O}(kR^3n^3)$, for $k = 1, 2$ [38].

5. Numerical Example

Our aim in this section is to numerically analyze the performance and benefits of the \mathbb{T}_k -proper LLMS centralized fusion filtering algorithm proposed in Theorem 1. Two examples are proposed: the first one, from simulated values, in which a scalar signal is estimated from the observations provided by several sensors; and the second one, a realistic model of a bidimensional tessarine state-space model which described a great amount of experimental phenomena. In both examples, by varying the Bernoulli parameters, different situations are compared in order to illustrate the effectiveness of the proposed algorithm in both \mathbb{T}_k -proper scenarios, for $k = 1, 2$.

5.1. Example 1

Consider the following multi-sensor tessarine state-space system:

$$\begin{aligned}x(t+1) &= F_1(t)x(t) + u(t), \quad t \geq 0, \\ z^{(i)}(t) &= x(t) + v^{(i)}(t), \quad t \geq 1, \\ y^{(i)}(t) &= \gamma^{(i)}(t) \star z^{(i)}(t) + (1 - \gamma^{(i)}(t)) \star y^{(i)}(t-1), \quad t \geq 2,\end{aligned} \quad (17)$$

for $i = 1, \dots, R$, with $y^{(i)}(1) = z^{(i)}(1)$, and where $F_1(t) = 0.3 + 0.3\eta + 0.1\eta' + 0.2\eta'' \in \mathbb{T}$. Moreover, $u(t)$ is a tessarine noise such that the covariance matrix of the associated real vector $\mathbf{u}^r(t)$ is of the form

$$\mathbf{\Gamma}_{\mathbf{u}^r}(t, s) = \begin{pmatrix} a & 0 & c & 0 \\ 0 & b & 0 & c \\ c & 0 & a & 0 \\ 0 & c & 0 & b \end{pmatrix} \delta_{t,s}, \quad (18)$$

where the parameters a , b and c take different values depending on the \mathbb{T}_k -proper scenario considered. Furthermore, to guarantee the correlation hypothesis between the state and observation noises, $u(t)$ and $v^{(i)}(t)$, they are assumed to satisfies the following expression:

$$v^{(i)}(t) = \alpha_i u(t) + w^{(i)}(t), \quad t \geq 1,$$

with $\alpha_i \in \mathbb{R}$, and where, at each i , $w^{(i)}(t)$ is a tessarine white Gaussian noise independent of $u(t)$, whose real covariance matrix is given by

$$\mathbf{\Gamma}_{\mathbf{w}^{(i)r}}(t, s) = \text{diag}(\beta_i, \beta_i, \beta_i, \beta_i), \quad t \geq 1,$$

Specifically, the following values of α_i and β_i , for $i = 1, 2, 3, 4, 5$, will be considered in our simulations:

$$\alpha_1 = 0.5, \alpha_2 = 0.3, \alpha_3 = 0.9, \alpha_4 = 0.6, \alpha_5 = 0.2$$

$$\beta_1 = 95, \beta_2 = 125, \beta_3 = 87, \beta_4 = 83, \beta_5 = 73$$

Additionally, the variance matrix of the real initial state $\mathbf{x}^r(0)$ is assumed to be of the form

$$\mathbf{\Gamma}_{\mathbf{x}^r}(0, 0) = \begin{pmatrix} d & 0 & f & 0 \\ 0 & e & 0 & f \\ f & 0 & d & 0 \\ 0 & f & 0 & e \end{pmatrix}, \quad (19)$$

whose values d , e and f will be specified in Section 5.1.1 and Section 5.1.2, according to the different \mathbb{T}_k -proper scenario analyzed.

5.1.1. \mathbb{T}_1 proper scenario

To guarantee that $x(t)$ and $y^{(i)}(t)$ are joint \mathbb{T}_1 -proper, it has been taken $a = b = 1$, $c = -0.5$ in (18) and $d = e = 4$, $c = 1.5$ in (19). Moreover, it has also been assumed that the components of the multiplicative noise in (17), $\gamma_\nu^{(i)}(t)$ have constant probabilities $p_\nu^{(i)} = p^{(i)}$, for all $\nu = r, \eta, \eta'\eta''$, and $i = 1, \dots, R$.

Firstly, the behavior of the estimators proposed is analyzed by considering a different number of sensors. Specifically, Figure 1 shows the \mathbb{T}_1 -proper centralized fusion filtering error variances computed from the observations provided by 2, 3, 4, and 5 sensors. As expected, it is the estimators perform better as the number of sensors increases, which makes sense because the number of observations used to estimate the signal increases.

Next, in order to show the computational savings attained with the solution proposed, under \mathbb{T}_1 -properness conditions, Table 1 presents the computation time required to apply the \mathbb{T}_1 -proper centralized fusion filtering algorithms given in Theorem 1, and the conventional one devised from a real-valued linear processing in the cases of 2, 3, 4, and 5 sensors. Then, a reduction in the computation time can be observed when the methodology proposed is used, and this computational saving becomes more significant as the number of sensors increases.

Our second objective is to compare tessarine and quaternion signal processing for different probabilities of updated/missing observations, under \mathbb{T}_1 -properness conditions. For this purpose, the error variances of both \mathbb{T}_1 and QSL centralized fusion filters have been calculated for the following cases:

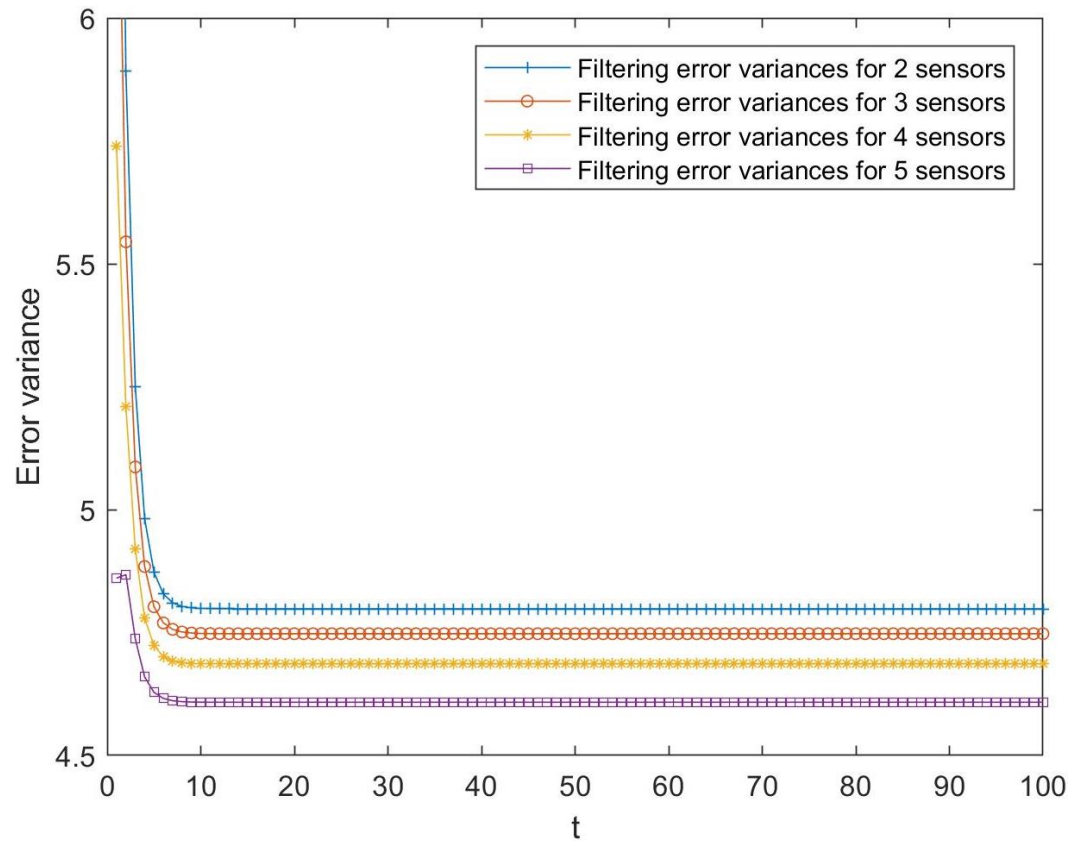


Figure 1. \mathbb{T}_1 proper centralized fusion filtering error variances with 2, 3, 4, and 5 sensors.

Table 1. Computation time (in seconds) for the \mathbb{T}_1 proper processing and the conventional one.

Type of processing	Number of sensors			
	2	3	4	5
\mathbb{T}_1 - proper	4.552597	9.328620	16.299967	25.112891
Real-valued	5.367786	10.935009	18.187468	27.570617

- Case 1: $p^{(i)} = 0.1, \forall i = 1, \dots, 5$;
- Case 2: $p^{(i)} = 0.3, \forall i = 1, \dots, 5$;
- Case 3: $p^{(i)} = 0.5, \forall i = 1, \dots, 5$;
- Case 4: $p^{(i)} = 0.7, \forall i = 1, \dots, 5$;
- Case 5: $p^{(i)} = 0.9, \forall i = 1, \dots, 5$.

Then, the difference between both tessarine and quaternion LLMS centralized fusion filtering error variances, that is, $D_1(t|t) = P_{QSL}(t|t) - P_1(t|t)$, have been computed and displayed in Figure 2. In this figure, positive differences can be observed in all the cases, meaning that it can be noted that \mathbb{T}_1 -proper fusion estimators perform better than their quaternion counterparts. As expected, the fact that the \mathbb{T}_1 -properness conditions are satisfied, determine that it is more appropriate to use the \mathbb{T}_1 -proper signal processing than the quaternion one, since it yields to better estimations. Moreover, these differences become smaller as the probability of updated observations increases.

Finally, with the aim of comparing both QSL and \mathbb{T}_1 -proper signal processing, they are applied by taking a fixed value for the probabilities of the Bernoulli parameters in all the sensors, but different values of c in (18), that is, $c = -0.8, -0.5, -0.2, 0$. Note that, for $c = 0$, the state additive noise, $u(t)$, is \mathbb{T}_1 besides \mathbb{Q} -proper, and as c is further away from 0, the \mathbb{Q} -properness conditions are further away. In this setting, the error variances of both

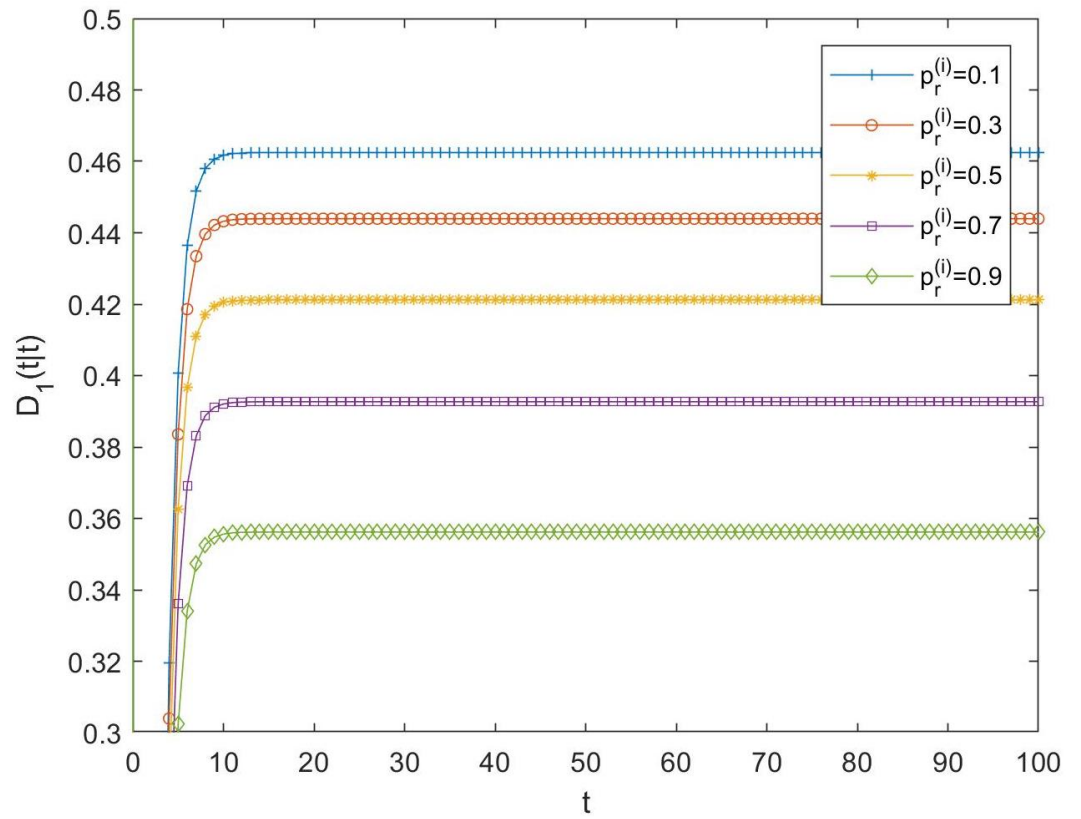


Figure 2. Difference $D_1(t|t)$ between QSL and \mathbb{T}_1 proper centralized fusion filtering error variances for cases 1, 2, 3, 4, and 5.

\mathbb{T}_1 -proper and QSL LLMS centralized fusion filters have been computed, and the mean of the differences between them, $MD_1(t|t) = \text{mean}(D_1(t|t))$, have been displayed in Figure 3 for the different values of c . In this figure, tessarine estimators are shown to be more accurate the further the noise $u(t)$ is from the \mathbb{Q} -properness conditions. Moreover, as in Figure 2, these differences decrease as the probability of updated observations increases.

5.1.2. \mathbb{T}_2 proper scenario

In order to guarantee \mathbb{T}_2 -properness conditions, $a = 1$, $b = 2$, $c = -0.5$ in (18) is assumed, and $d = 4$, $e = 3$, $c = 1.5$ in (19), and also $p_r^{(i)} = p_{\eta'}^{(i)}$, and $p_{\eta''}^{(i)} = p_{\eta'''}^{(i)}$, for $i = 1, \dots, 5$.

As in the previous subsection, in order to compare the performance of tessarine and quaternion processing under \mathbb{T}_2 -properness conditions, the differences between the LLMS centralized fusion filtering error variances of the QSWL and \mathbb{T}_2 -proper estimators, denoted by $D_2(t|t)$, have been computed and displayed in Figure 4, for the following cases:

- Case 6: $p_r^{(i)} = 0.1$ and $p_{\eta'}^{(i)} = 0.2$, $\forall i = 1, \dots, 5$;
- Case 7: $p_r^{(i)} = 0.3$ and $p_{\eta'}^{(i)} = 0.4$, $\forall i = 1, \dots, 5$;
- Case 8: $p_r^{(i)} = 0.5$ and $p_{\eta'}^{(i)} = 0.6$, $\forall i = 1, \dots, 5$;
- Case 9: $p_r^{(i)} = 0.7$ and $p_{\eta'}^{(i)} = 0.8$, $\forall i = 1, \dots, 5$;
- Case 10: $p_r^{(i)} = 0.9$ and $p_{\eta'}^{(i)} = 1$, $\forall i = 1, \dots, 5$.

Because these differences are positive in all the cases, the superiority of the \mathbb{T}_2 -proper tessarine processing over the QSWL processing under \mathbb{T}_2 -properness conditions is clear, and these differences become smaller as the probability that the components of the available observation are updated increases.

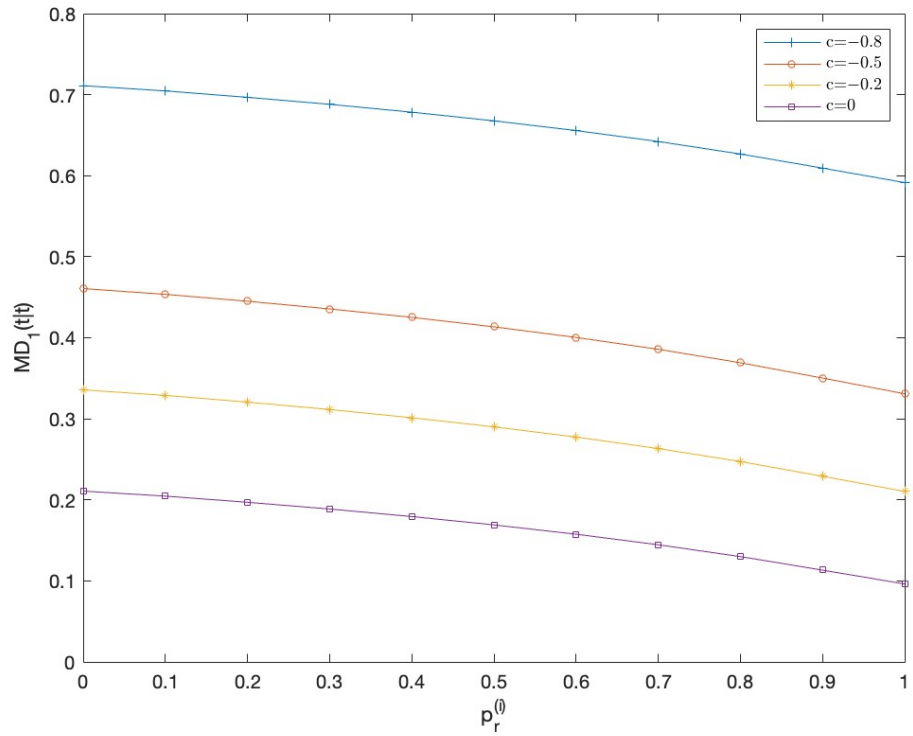


Figure 3. Mean of the differences $MD_1(t|t)$ between QSL and \mathbb{T}_1 proper centralized fusion filtering error variances.

5.2. Example 2

Let us consider the following general equation of motion [33]:

$$\frac{\partial \varphi}{\partial t} = \phi, \quad \text{and} \quad \frac{\partial \phi}{\partial t} = v, \quad (20)$$

where φ is the variable of interest, ϕ its range of change, and v the input of the system.

Notice that equation (20) models a great amount of physical phenomena and it has been used, for example, in bearing-only tracking applications and rotation tracking problems, where v represents, respectively, the force or acceleration and the torque or angular acceleration.

In discrete-time, by taking $\mathbf{x}(t) = [\varphi(t), \phi(t)]^T$, it is possible to build a model equivalent to that given in (20), as follows:

$$\begin{aligned} \mathbf{x}(t+1) &= \begin{pmatrix} 1 & 0.04 \\ 0 & 1 \end{pmatrix} \mathbf{x}(t) + \begin{bmatrix} 0.0008 \\ 0.04 \end{bmatrix} \varpi(t), \quad t = 1, \dots, 100; \\ \mathbf{x}(0) &= \mathbf{0}_{2 \times 1}, \end{aligned}$$

where $\varpi(t)$ is a tessarine white noise with real covariance matrix:

$$E[\varpi^r(t) \varpi^{r^T}(s)] = \begin{pmatrix} 3 & 0 & 2 & 0 \\ 0 & 3 & 0 & 2 \\ 2 & 0 & 3 & 0 \\ 0 & 2 & 0 & 3 \end{pmatrix} \delta_{ts}, \quad t, s = 1, \dots, 100.$$

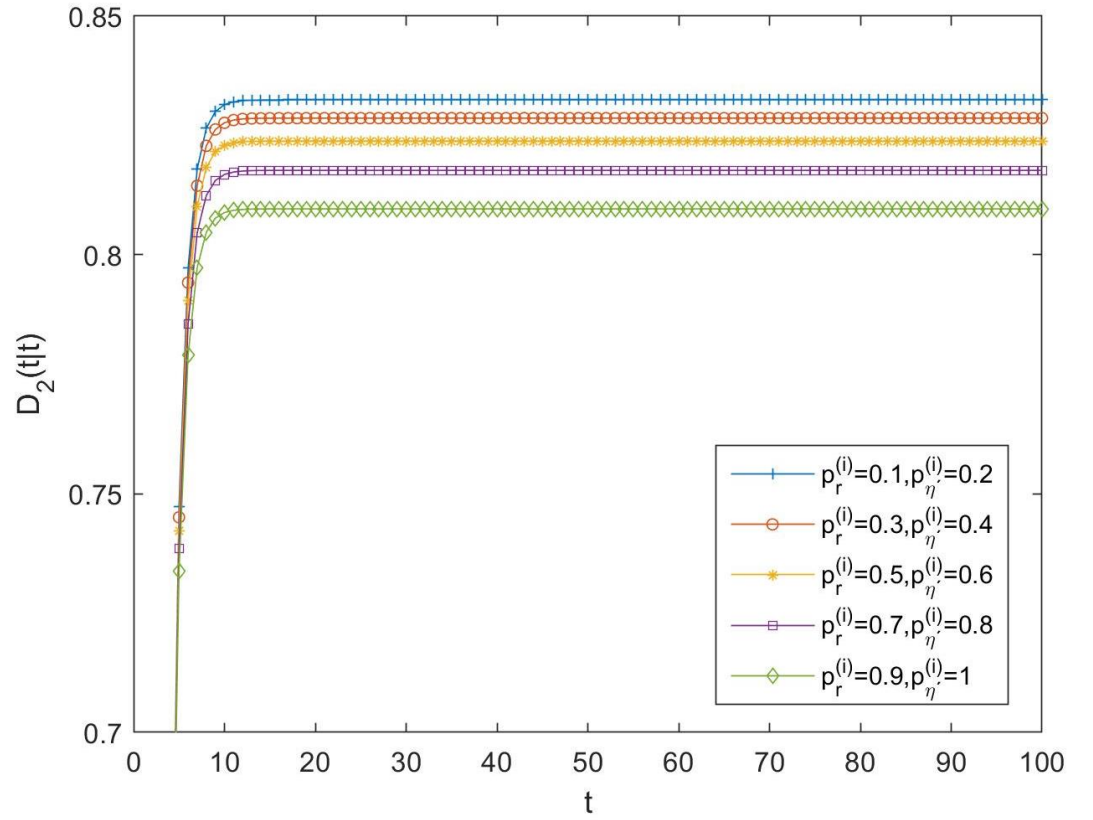


Figure 4. Difference $D_2(t|t)$ between QSWL and \mathbb{T}_2 proper centralized fusion filtering error variances for cases 6, 7, 8, 9, and 10.

Moreover, the additive noise of single-sensor real observation equation, $\mathbf{v}(t) = [v_1(t), v_2(t)]^T$, is assumed to be a tessarine white noise with independent components and associated real covariance matrices given by

$$E[\mathbf{v}_j^r(t) \mathbf{v}_j^{r^T}(s)] = \begin{pmatrix} 6.5 & 0 & 0.1 & 0 \\ 0 & 6.5 & 0 & 0.1 \\ 0.1 & 0 & 6.5 & 0 \\ 0 & 0.1 & 0 & 6.5 \end{pmatrix} \delta_{ts}, \quad t, s = 1, \dots, 100, \quad j = 1, 2.$$

In order to guarantee the \mathbb{T}_k -properness conditions, the following assumptions and cases about the parameters of the Bernoulli random variables have been considered:

- In the \mathbb{T}_1 -proper scenario: $p_{j,\nu}(t) = p_j$, for all $j = 1, 2$, $\nu = r, \eta, \eta' \eta''$:
 - Case 11: $p_1 = 0.1$, $p_2 = 0.2$;
 - Case 12: $p_1 = 0.3$, $p_2 = 0.4$;
 - Case 13: $p_1 = 0.5$, $p_2 = 0.6$;
 - Case 14: $p_1 = 0.7$, $p_2 = 0.8$;
 - Case 15: $p_1 = 0.9$, $p_2 = 1$.
- In the \mathbb{T}_2 -proper scenario: $p_{j,r}(t) = p_{j,\nu}(t) = p_{j,r}$, $p_{j,\eta'}(t) = p_{j,\nu''}(t) = p_{j,\eta'}$, for all $j = 1, 2$:
 - Case 16: $p_{1,r} = 0.1$, $p_{1,\eta'} = p_{2,r} = 0.2$, $p_{2,\eta'} = 0.3$;
 - Case 17: $p_{1,r} = 0.3$, $p_{1,\eta'} = p_{2,r} = 0.4$, $p_{2,\eta'} = 0.5$;
 - Case 18: $p_{1,r} = 0.5$, $p_{1,\eta'} = p_{2,r} = 0.6$, $p_{2,\eta'} = 0.7$;
 - Case 19: $p_{1,r} = 0.7$, $p_{1,\eta'} = p_{2,r} = 0.8$, $p_{2,\eta'} = 0.9$;
 - Case 20: $p_{1,r} = 0.9$, $p_{1,\eta'} = p_{2,r} = 0.95$, $p_{2,\eta'} = 1$.

For all the above cases, the differences between the quaternion and tessarine filtering error variances have been calculated and displayed in Figures 5 and 6, for the \mathbb{T}_1 and \mathbb{T}_2 -proper scenarios and for the first and second component of the signal, respectively. Same conclusions can be derived for both figures: 1) better estimations by using the tessarine processing than from the quaternion processing and, 2) there exists a lower difference between the estimations obtained from both types of processing when the probability that the components of the available observations are updated increases.

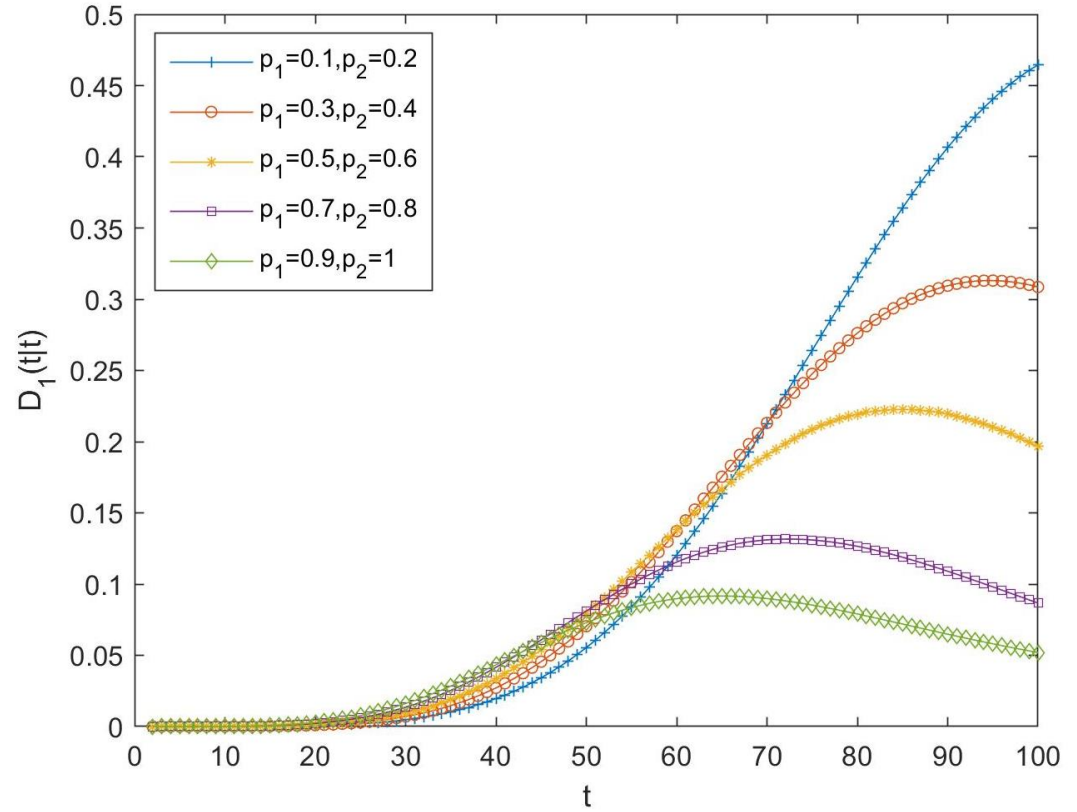


Figure 5. Difference $D_1(t|t)$ between QSL and \mathbb{T}_1 proper fusion filtering error variances for the first component of the signal for cases 11, 12, 13, 14, and 15.

6. Discussion

The LLMS centralized fusion filtering problem is analyzed in linear systems with multiple sensors and multiple packet dropouts. However, unlike most of the solutions proposed in the literature, a proper hypercomplex-valued signal processing has been employed with the purpose of reducing the dimension of the problem. Specifically, the state-space system is defined in the tessarine domain, and it is assumed that each component of the measurement output at each sensor may present a different packet dropout rate, modeled by using a Bernoulli random variable. Moreover, the state and the measurement noises can be correlated. Under hypotheses of \mathbf{T}_k -properness, our approach allows us to provide an optimal LLMS fusion filtering algorithm that reduces the computational cost of its counterpart in the real field. The good behavior and benefits of this algorithm has been analyzed in situations of \mathbf{T}_1 and \mathbf{T}_2 -properness, by considering different number of sensors. Moreover, a comparative study of the quaternion and tessarine approaches has been carried out, showing how the algorithm proposed behaves better than its counterpart in the quaternion domain when \mathbf{T}_k -properness, $k = 1, 2$, conditions are satisfied.

As a consequence, our approach based on \mathbf{T}_k -proper processing presents two main advantages: on the one hand, the tessarine systems offers a suitable framework to model 3D and 4D physical and experimental phenomena, and on the other hand, a considerably

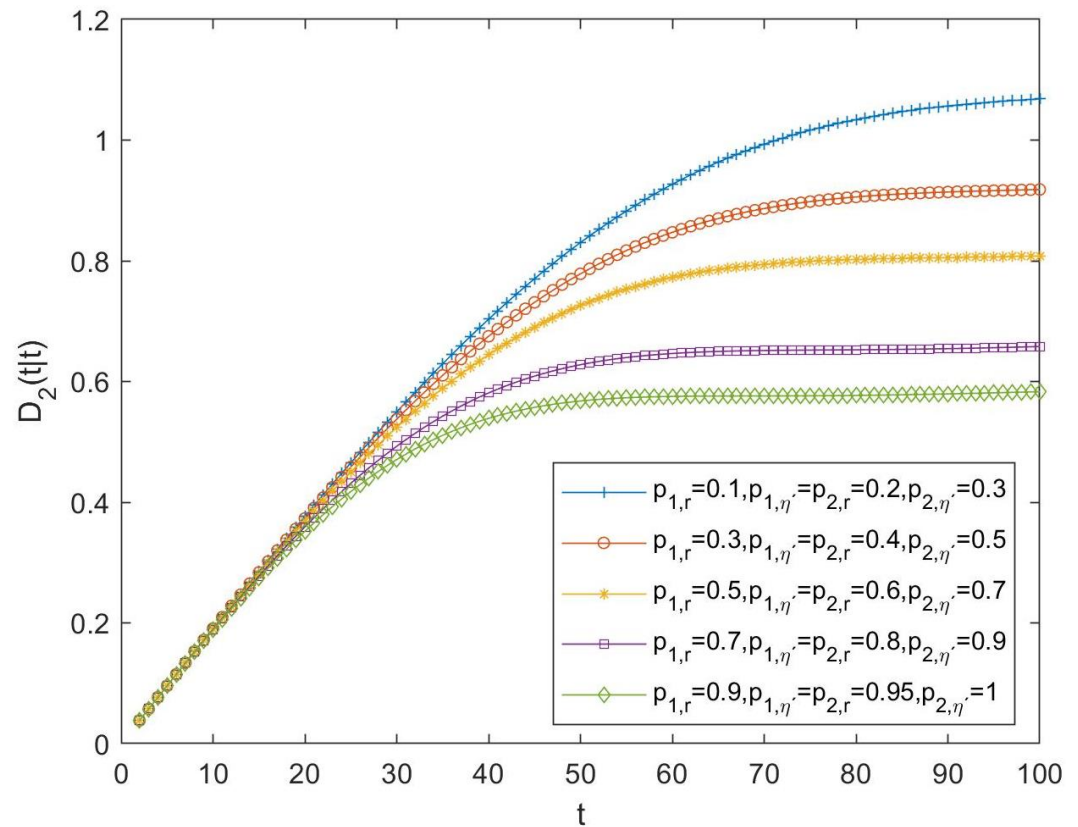


Figure 6. Difference $D_2(t|t)$ between QSWL and T_2 proper fusion filtering error variances for the second component of the signal for cases 16, 17, 18, 19, and 20.

reduction of problem dimension is possible, when the processes involved are T_k -proper, which implies significant computational savings in the implementation of our LLMS fusion filtering algorithm, that cannot be attained from a real formalism of the problem.

In future research, we will approach the estimation problem in other hypercomplex algebras and under different properness conditions, by using alternative fusion architectures for the multi-sensor observations, and with varied uncertainty situations.

Author Contributions: All authors have contributed equally to the work. The functions mainly carried out by each specific author are detailed below. Conceptualization, R.M.F.-A., N.L.-B., and C.C.T.; formal analysis, R.M.F.-A., and J.D.J.-L.; methodology, R.M.F.-A., J.D.J.-L.; investigation, R.M.F.-A., and J.D.J.-L.; visualization, R.M.F.-A., J.D.J.-L., N.L.-B., and C.C.T.; writing—original draft preparation, R.M.F.-A. and J.D.J.-L.; writing—review and editing, R.M.F.-A., J.D.J.-L., N.L.-B., and C.C.T.; funding acquisition, R.M.F.-A. and J.D.J.-L.; project administration, R.M.F.-A.; software, J.D.J.-L.; supervision, R.M.F.-A., J.D.J.-L., N.L.-B., and C.C.T.; validation, R.M.F.-A., J.D.J.-L., N.L.-B., and C.C.T. All authors have read and agreed to the published version of the manuscript.

Funding: This paper has been supported in part by the Project PID2021-124486NB-I00 of the Plan Estatal de I+D+i", Ministerio de Educación y Ciencia, Spain, the I+D+i project with reference number 1256911, under 'Programa Operativo FEDER Andalucía 2014–2020', Junta de Andalucía, and Project EI-FQM2-2023 of 'Plan de Apoyo a la Investigación 2023–2024' from the University of Jaén.

Institutional Review Board Statement: Not applicable.

Informed Consent Statement: Not applicable.

Data Availability Statement: Not applicable.

Conflicts of Interest: The authors declare no conflict of interest.

Abbreviations

The following abbreviations are used in this manuscript:

LLMS	Linear least-mean-squares
QSL	Quaternion strictly linear
QSWL	Quaternion semi-widely linear
WL	Widely linear

Appendix A. Proof of Theorem 1

Consider the state-space system given by the equations (3)-(4), and (6). On the basis of the innovations $\varepsilon_k(t) = \mathbf{y}_k(t) - \hat{\mathbf{y}}_k(t|t-1)$, with $\hat{\mathbf{y}}_k(t|t-1)$ the LLMS estimator of $\mathbf{y}_k(t)$ based on the measurements $\{\mathbf{y}_k(1), \dots, \mathbf{y}_k(t-1)\}$, for $k = 1, 2$, the LLMS filter $\hat{\mathbf{x}}(t|t)$ of $\bar{\mathbf{x}}(t)$ can be expressed as [36]:

$$\hat{\mathbf{x}}(t|t) = \sum_{s=1}^t \bar{\mathbf{\Theta}}_k(s) \mathbf{\Omega}_k^{-1}(s) \varepsilon_k(s),$$

where $\bar{\mathbf{\Theta}}_k(s) = E[\bar{\mathbf{x}}(s) \varepsilon_k^H(s)]$, and $\mathbf{\Omega}_k(s) = E[\varepsilon_k(s) \varepsilon_k^H(s)]$, which yields the recursive equation

$$\hat{\mathbf{x}}(t|t) = \hat{\mathbf{x}}(t|t-1) + \bar{\mathbf{L}}_k(t) \varepsilon_k(t), \quad (\text{A1})$$

with $\bar{\mathbf{L}}_k(t) = \bar{\mathbf{\Theta}}_k(t) \mathbf{\Omega}_k^{-1}(t)$. Thus, from the \mathbb{T}_k -properness conditions, the equation (8) is obtained.

Moreover, taking projections on both sides of equations (3) and (5), we obtain that

$$\hat{\mathbf{x}}(t+1|t) = \bar{\mathbf{\Phi}}(t) \hat{\mathbf{x}}(t|t) + \bar{\mathbf{H}}_k(t) \varepsilon_k(t), \quad (\text{A2})$$

with $\bar{\mathbf{H}}_k(t) = \bar{\mathbf{S}}(t) \bar{\mathbf{\Pi}}_k^{\tilde{\gamma}^H}(t) \mathbf{\Omega}_k^{-1}(t)$, and

$$\hat{\mathbf{y}}_k(t|t-1) = \bar{\mathbf{\Pi}}_k^{\tilde{\gamma}}(t) \mathbf{C} \hat{\mathbf{x}}(t|t-1) + \bar{\mathbf{\Pi}}_k^{(1-\tilde{\gamma})}(t) \bar{\mathbf{y}}_k(t-1), \quad (\text{A3})$$

Then, by applying \mathbb{T}_k -properness conditions on (A2) and (A3), and considering that $E[\bar{\mathbf{u}}(t) \varepsilon_k^H(s)] = \bar{\mathbf{S}}(t) \bar{\mathbf{\Pi}}_k^{\tilde{\gamma}^H}(t) \delta_{t,s}$, the equations (9) and (10) are directly devised.

Let $\bar{\mathbf{e}}(t|t-1) = \bar{\mathbf{x}}(t) - \hat{\mathbf{x}}(t|t-1)$ be the prediction error, then

$$\bar{\mathbf{\Theta}}_k(t) = E[\bar{\mathbf{x}}(t) \varepsilon_k^H(t|t-1)] \mathbf{C}^T \bar{\mathbf{\Pi}}_k^{\tilde{\gamma}^H}(t) = \bar{\mathbf{P}}(t|t-1) \mathbf{C}^T \bar{\mathbf{\Pi}}_k^{\tilde{\gamma}^H}(t), \quad t \geq 2,$$

where $\bar{\mathbf{P}}(t|t-1) = E[\bar{\mathbf{e}}(t|t-1) \bar{\mathbf{e}}^H(t|t-1)]$. As a consequence, under \mathbb{T}_k -properness conditions, (11) is derived, where $\mathbf{P}_k(t|t-1)$ is given by the first $knR \times knR$ submatrix of $\bar{\mathbf{P}}(t|t-1)$ and also the equation (13) for $\mathbf{\Gamma}_{\bar{\mathbf{x}}}(t) = E[\bar{\mathbf{x}}(t) \bar{\mathbf{x}}^H(t)]$ is easily obtained from (3).

In order to devise the equation (14), we will rewrite the equation (10) as follows:

$$\varepsilon_k(t) = \Delta \bar{\mathcal{D}}_k^{\tilde{\gamma}}(t) \mathbf{C} \bar{\mathbf{x}}(t) + \bar{\mathbf{\Pi}}_k^{\tilde{\gamma}}(t) \mathbf{C} \bar{\mathbf{e}}(t|t-1) + \bar{\mathcal{D}}_k^{\tilde{\gamma}}(t) \bar{\mathbf{v}}(t) + \Delta \bar{\mathcal{D}}_k^{(1-\tilde{\gamma})}(t) \bar{\mathbf{y}}(t-1).$$

Then, considering that $\bar{\mathbf{v}}(t)$ is orthogonal to $\bar{\mathbf{x}}(t)$, $\bar{\mathbf{y}}(t-1)$, and $\bar{\mathbf{e}}(t|t-1)$, and $E[\Delta \bar{\mathcal{D}}_k^{\tilde{\gamma}}(t)] = 0$, we have that

$$\begin{aligned} \mathbf{\Omega}_k(t) = & E \left[\Delta \bar{\mathcal{D}}_k^{\tilde{\gamma}}(t) \mathbf{C} \bar{\mathbf{x}}(t) \bar{\mathbf{x}}^H(t) \mathbf{C}^T \Delta \bar{\mathcal{D}}_k^{\tilde{\gamma}^H}(t) \right] + E \left[\Delta \bar{\mathcal{D}}_k^{\tilde{\gamma}}(t) \mathbf{C} \bar{\mathbf{x}}(t) \bar{\mathbf{y}}^H(t-1) \Delta \bar{\mathcal{D}}_k^{(1-\tilde{\gamma})^H}(t) \right] \\ & + E \left[\Delta \bar{\mathcal{D}}_k^{(1-\tilde{\gamma})}(t) \bar{\mathbf{y}}(t-1) \bar{\mathbf{x}}^H(t) \mathbf{C}^T \Delta \bar{\mathcal{D}}_k^{\tilde{\gamma}^H}(t) \right] + E \left[\bar{\mathcal{D}}_k^{\tilde{\gamma}}(t) \bar{\mathbf{v}}(t) \bar{\mathbf{v}}^H(t) \bar{\mathcal{D}}_k^{\tilde{\gamma}^H}(t) \right] \\ & + E \left[\Delta \bar{\mathcal{D}}_k^{(1-\tilde{\gamma})}(t) \bar{\mathbf{y}}(t-1) \bar{\mathbf{y}}^H(t-1) \Delta \bar{\mathcal{D}}_k^{(1-\tilde{\gamma})^H}(t) \right] + \bar{\mathbf{\Pi}}_k^{\tilde{\gamma}}(t) \mathbf{C} \bar{\mathbf{P}}(t|t-1) \mathbf{C}^T \bar{\mathbf{\Pi}}_k^{\tilde{\gamma}^H}(t). \end{aligned} \quad (\text{A4})$$

The equation (14) follows from (A4), by using Hadamard product properties and taking into account that

$$\Gamma_{\bar{\mathbf{x}}\bar{\mathbf{y}}}(t, t-1) = \bar{\Phi}(t-1)\Gamma_{\bar{\mathbf{x}}\bar{\mathbf{y}}}(t-1) + \bar{\mathbf{S}}(t-1)\bar{\Pi}^{\bar{\gamma}}(t-1).$$

Finally, from (A1), it is clear that the pseudo covariance matrix $\bar{\mathbf{P}}(t|t) = E[\bar{\epsilon}(t|t)\bar{\epsilon}^H(t|t)]$, of the filtering errors $\bar{\epsilon}(t|t) = \bar{\mathbf{x}}(t) - \hat{\mathbf{x}}(t|t)$, can be computed of the form

$$\bar{\mathbf{P}}(t|t) = \bar{\mathbf{P}}(t|t-1) - \bar{\Theta}_k(t)\bar{\Omega}_k^{-1}(t)\bar{\Theta}_k^H(t),$$

and consequently, using the \mathbb{T}_k properness conditions, (15) holds. Furthermore, since

$$\bar{\epsilon}(t+1|t) = \bar{\mathbf{x}}(t+1) - \hat{\mathbf{x}}(t+1|t) = \bar{\Phi}(t)\bar{\epsilon}(t|t) + \bar{\mathbf{u}}(t) - \bar{\mathbf{H}}_k(t)\bar{\epsilon}_k(t), \quad (\text{A5})$$

$E[\bar{\epsilon}(t|t)\bar{\epsilon}_k(t)] = 0$, and $E[\bar{\mathbf{u}}(t)\bar{\epsilon}^H(t|t)] = -\bar{\mathbf{S}}(t)\bar{\Pi}_k^{\bar{\gamma}}(t)\bar{\mathbf{L}}_k^H(t)$, we obtain that

$$\begin{aligned} \bar{\mathbf{P}}(t+1|t) &= \bar{\Phi}(t)\bar{\mathbf{P}}(t|t)\bar{\Phi}^H(t) - \bar{\mathbf{H}}_k(t)\bar{\Theta}_k^H(t)\bar{\Phi}^H(t) \\ &\quad - \bar{\Phi}(t)\bar{\Theta}_k(t)\bar{\mathbf{H}}_k^H(t) - \bar{\mathbf{H}}_k(t)\bar{\Omega}_k(t)\bar{\mathbf{H}}_k^H(t) + \bar{\mathbf{Q}}(t), \end{aligned}$$

and hence, from \mathbb{T}_k properness conditions, (16) follows.

References

1. Kurkin, A. A.; Tyugin, D. Y.; Kuzin, V. D.; Chernov, A. G.; Makarov, V. S.; Beresnev, P. O.; Filatov, V. I.; Zeziulin, D. V. Autonomous mobile robotic system for environment monitoring in a coastal zone. *Procedia Comput. Sci.* **2017**, *103*, 459–465.
2. Kondru, D. S.R.; Celenk, M.; Shen, X. State estimation-based target tracking and applications of multi sensor data fusion. *Int. J. of Forensic Soft. Eng.* **2017**, *1* (32). doi: 10.1504/IJFSE.2019.104718.
3. Huang, S. ; Chou, P. . ; Jin, X. ; Zhang, Y. ; Jiang, Q. ; Yao, S. Multi-sensor image fusion using optimized support vector machine and multiscale weighted principal component analysis. *Electronics* **2020**, *9* (9), 1531. <https://doi.org/10.3390/electronics9091531>.
4. Liping, Y.; Xia, Y.; Jiang, L. *Multisensor Fusion Estimation Theory and Application*; 1st ed.; Springer: Gateway East, Singapore, 2021.
5. Tian, C.; Leng, B.; Hou, X.; Xiong, L.; Huang, C. Multi-sensor fusion based estimation of tire-road peak adhesion coefficient considering model uncertainty. *Remote Sens.* **2022**, *14*, 5583. <https://doi.org/10.3390/rs14215583>.
6. Kong, D.; Li, X.; Hu, Y.; Xu, Q.; Wang, A.; Hu, W. Learning a novel LiDAR submap-based observation model for global positioning in long-term changing environments. *IEEE Trans. Ind. Electron.* **2023**, *70* (3), 3147–3157. <https://doi.org/10.1109/TIE.2022.3169849>.
7. Zewge, N.S.; Bang, H. A distributionally robust fusion framework for autonomous multisensor spacecraft navigation during entry phase of mars entry, descent, and landing. *Remote Sens.* **2023**, *15* (4), 1139. <https://doi.org/10.3390/rs15041139>.
8. Zheng, J.; Ran, C. Distributed fusion robust estimators for multisensor networked singular control system with uncertain-variance correlated noises and missing measurement. *Comput. Appl. Math.* **2023**, *42* (1), 66. <https://doi.org/10.1007/s40314-023-02202-3>.
9. Liu, W.-Q.; Liu, W.; Li, S.; Tao, G.-L. Fusion steady-state robust filtering for uncertain multisensor networked systems with application to autoregressive moving average signal estimates. *Optim. Control Appl. Methods* **2023**, *44* (1), 275–307. <https://doi.org/10.1002/oca.2950>.
10. Schenato, L. Optimal sensor fusion for distributed sensors subject to random delay and packet loss. 46th IEEE Conference on Decision and Control, New Orleans, LA, USA, **2007**, 1547–1552. doi: 10.1109/CDC.2007.4434360.
11. Sun, S.; Xie, L.; Xiao, W.; Soh, Y.C. Optimal linear estimation for systems with multiple packet dropouts. *Automatica* **2008**, *44*, 1333–1342.
12. Sun, S.; Ma, J. Linear estimation for networked control systems with random transmission delays and packet dropouts. *Inf. Sci.* **2014**, *269*, 349–365.
13. Zhao, H.; Wang, T.; Jin, H.; Ma, J. Zero-input compensation mechanism-based linear estimation for systems with multiple packet dropouts and multiplicative noises. *Int. J. Signal Process. Image Process. Pattern Recogn.* **2016**, *9* (11), 331–340.
14. Lu, Z.; Zhong, S.; Qu, L. A switching approach to packet loss compensation strategy, . *IEEE Access.* **2019**, *7*, 5609–5615. doi: 10.1109/ACCESS.2018.2888518.
15. Song, X.; Wei, D.; Chen, Y.; Zhu, W. Bidirectional asymmetric delay feedback for cooperative adaptive cruise control of vehicle platoons with unreliable communication, *Asian J. Control*, **2022**, *24* (6), 3066–3079. doi: 10.1002/asjc.2702.
16. Li, B.; Zhou, X.; Ning, Z.; Guan, X.; Yiu, K.-F.C. Dynamic event-triggered security control for networked control systems with cyber-attacks: A model predictive control approach, *Information Sciences*, **2022**, *612*, 384–398. doi: 10.1016/j.ins.2022.08.093.

17. Su, Y.; Hu, Z.; Chen, K.; Luo, T.; Li, Y. State Feedback Controller Design of Networked Sampled-Data Systems with Packet Loss, *Int. J. Innov. Comput. Inf. Control.*, **2022**, *18* (4), 1305–1316. doi: 10.24507/ijicic.18.04.1305.
18. Geng, Q.; Zhao, L.; Li, L.; Liu, F. A dynamic controller design for trajectory tracking control of wheeled mobile robot under stochastic denial of service attacks, *IEEE Trans. Circuits Syst. II Express Briefs*, **2022**, *69* (8), 3560–3564. doi: 10.1109/TCSII.2022.3168304.
19. Xu, Y.; Pan, M.; Huang, J.; Zhou, W.; Qiu, X. An intelligent estimation-based large-scale envelope control for variable cycle engine with packet dropout, *Aerosp. Sci. Technol.* **2023**, *133*, 108078. doi: <https://doi.org/10.1016/j.ast.2022.108078>.
20. Zhu, X.; Zhang, X.; Wei, J.; Lin, H. Output-based dynamic event-triggered control for networked control systems with delays and packet losses without acknowledgements, *IEEE Trans. Automat. Contr.* **2023**, 1–16. doi: 10.1109/TAC.2023.3250030.
21. Ni, J.; Zhao, Y. Fixed-time consensus tracking of wheeled mobile robots under digraph with packet dropout, *Lect. Notes Electr. Eng.*, **2023**, *934*, 1455–1467. doi: 10.1007/978-981-19-3998-3_136.
22. Elahi, A.; Alfi, A.; Modares, H. Distributed consensus control of vehicular platooning under delay, packet dropout and noise: Relative state and relative input-output control strategies, *IEEE Trans. Intell. Transp. Syst.*, **2023**, *23* (11), 20123–20133. doi: 10.1109/TITS.2022.3174060.
23. Ma, J.; Sun, S. Information fusion estimators for systems with multiple sensors of different packet dropout rates. *Inf. Fusion* **2011**, *12* (3), 213–222. <https://doi.org/10.1016/j.inffus.2010.11.003>
24. Caballero-Águila, R.; Hermoso-Carazo, A.; Linares-Pérez, J. Least-squares linear estimators using measurements transmitted by different sensors with packet dropouts. *Digit. Signal Process.* **2012**, *22* (6), 1118–1125. <https://doi.org/10.1016/j.dsp.2012.06.002>.
25. Ma, J.; Sun, S. Centralized fusion estimators for multisensor systems with random sensor delays, multiple packet dropouts and uncertain observations. *IEEE Sens. J.* **2013**, *13* (4), 1228–1235.
26. Li, N.; Sun, S.; Ma, J. Multi-sensor distributed fusion filtering for networked systems with different delay and loss rates. *Digit. Signal Process.* **2014**, *34*, 29–38.
27. Li, S.; Liu, W.; Guili, T. Centralized fusion robust filtering for networked uncertain systems with colored noises, one-step random delay, and packet dropouts. *EURASIP J. Adv. Signal Process.* **2022**, *2022*: 24, 1–23. DOI:10.1186/s13634-022-00857-4
28. Yuan, X.; Yu, S.; Zhang, S.; Wang, G.; Liu, S. Quaternion-Based Unscented Kalman Filter for Accurate Indoor Heading Estimation Using Wearable Multi-Sensor System. *Sensors* **2015**, *15*, 10872–10890. <https://doi.org/10.3390/s150510872>
29. Talebi, S.; Kanna, S.; Mandic, D. A distributed quaternion Kalman filter with applications to smart grid and target tracking, *IEEE Trans. Signal Inf. Process. Networks* **2016**, *2*, 477–488.
30. Tannous, H.; Istrate, D.; Benlarbi-Delai, A.; Sarrazin, J.; Gamet, D.; Ho Ba Tho, M. C.; Dao, T. T. A new multi-sensor fusion scheme to improve the accuracy of knee flexion kinematics for functional rehabilitation movements, *J. Sensors* **2016**, *16* (11), 1914.
31. Navarro-Moreno, J.; Fernández-Alcalá, R. M.; Jiménez López, J. D.; Ruiz-Molina, J. C. Widely linear estimation for multisensor quaternion systems with mixed uncertainties in the observations, *J. Frankl. Inst.* **2019**, *356*, 3115–3138.
32. Wu, J.; Zhou, Z.; Fourati, H.; Li, R.; Liu, M. Generalized linear quaternion complementary filter for attitude estimation from multi-sensor observations: An optimization approach. *IEEE Trans. Autom. Sci. Eng.* **2019**, *16*, 1330–1343.
33. Talebi, S. P.; Werner, S.; Mandic, D. P. Quaternion-valued distributed filtering and control, *IEEE Trans. Autom. Control.* **2020**, *65* (10), 4246–4256.
34. Fernández-Alcalá, R. M.; Navarro-Moreno, J.; Ruiz-Molina, J. C. \mathbb{T} -proper hypercomplex centralized fusion estimation for randomly multiple sensor delays systems with correlated noises. *Sensors* **2021**, *21*, 5729.
35. Jiménez-López, J. D.; Fernández-Alcalá, R. M.; Navarro-Moreno, J.; Ruiz-Molina, J. C., The distributed and centralized fusion filtering problems of tessarine signals from multi-sensor randomly delayed and missing observations under \mathbb{T}_k -properness conditions. *Mathematics* **2021**, *9*, 2961. <https://doi.org/10.3390/math922961>.
36. Navarro-Moreno, J.; Fernández-Alcalá, R. M.; Jiménez-López, J. D. and Ruiz-Molina, J. C., Tessarine signal processing under the \mathbb{T} -properness condition. *J. Franklin Inst.* **2020**, *357* (14), 10100–10126.
37. Navarro-Moreno, J. ; Ruiz-Molina, J. C. Wide-sense Markov signals on the tessarine domain. A study under properness conditions. *Signal Process.* **2021**, *183*, 108022.
38. Nitta, T.; Kobayashi, M.; Mandic, D. P. Hypercomplex widely linear estimation through the lens of underpinning geometry. *IEEE Trans. Signal Process.* **2019**, *67*, 3985–3994.